A Letters Journal Exploring the Frontiers of Physics

February 2017

EPL, **117** (2017) 35001
doi: 10.1209/0295-5075/117/35001

www.epljournal.org

Experimental observation of parametric instabilities at laser intensities relevant for shock ignition

G. Cristoforetti[1], A. Colaïtis[2], L. Antonelli[3], S. Atzeni[3], F. Baffigi[1], D. Batani[2,4], F. Barbato[5], G. Boutoux[2], R. Dudzak[6], P. Koester[1], E. Krousky[6], L. Labate[1], Ph. Nicolaï[2], O. Renner[7], M. Skoric[8], V. Tikhonchuk[2] and L. A. Gizzi[1]

[1] *Intense Laser Irradiation Laboratory, INO CNR (National Council of Research) - Pisa, Italy*
[2] *Université de Bordeaux, CNRS, CEA, CELIA (Centre Lasers Intenses et Applications) - Talence, France*
[3] *Dipartimento SBAI, Università di Roma "La Sapienza" - Rome, Italy*
[4] *National Research Nuclear University MEPhI, Department of Plasma Physics - Moscow, Russia*
[5] *Empa Swiss Federal Laboratories for Materials Science and Technology - Dübendorf, Switzerland*
[6] *Prague Asterix Laser System - Prague, Czech Republic*
[7] *Institute of Physics & ELI Beamlines, ASCR - Prague, Czech Republic*
[8] *Vinca Institute of Nuclear Sciences - Belgrade, Serbia*

received 11 January 2017; accepted in final form 15 March 2017
published online 31 March 2017

PACS 52.38.-r – Laser-plasma interactions
PACS 52.38.Dx – Laser light absorption in plasmas (collisional, parametric, etc.)
PACS 52.65.-y – Plasma simulation

Abstract – We report measurements of parametric instabilities and hot electron generation in a laser intensity regime up to $6 \times 10^{15}\,\mathrm{W/cm^2}$, typical of the shock ignition approach to inertial fusion. Experiments performed at the PALS laboratory in Prague show that the incident laser energy losses are dominated by Stimulated Brillouin Scattering (SBS) rather than by Stimulated Raman Scattering (SRS) or Two-Plasmon Decay (TPD). Results are compared to hydrodynamics simulations using a code that includes self-consistent calculations of non-linear laser plasma interactions and accounts for the laser intensity statistics contained in the beam speckles. Good agreement is found for the backscattered SRS light, and for temperature and flux of hot electrons. The effect of high-intensity speckles on backscattered SRS is also underlined numerically and experimentally.

Introduction. – Shock Ignition (SI) [1–6] is a promising approach to Inertial Confinement Fusion (ICF) [7–9], that relies on the separation of the compression and ignition phases. Since the target is not meant to be ignited by the pressure-volume work of the imploding capsule, it can be assembled at lower velocities [1] with lower intensity nanosecond laser pulses ($I \approx 5 \times 10^{14}\,\mathrm{W/cm^2}$). This reduces the risks associated to hydrodynamic instabilities during the compression. The ignition of the hotspot relies on an intense laser pulse (I up to $\approx 10^{16}\,\mathrm{W/cm^2}$), generating a pressure $P > 300\,\mathrm{Mbar}$ at the ablation layer which drives a strong shock into the target. The final fuel assembly is non-isobaric resulting in higher target gains than in conventional hotspot ignition. This scheme is compatible with present-day "NIF-like" laser technology [2,10,11] and, therefore, a full-scale demonstration of SI could be realized in the next decade.

The success of the SI concept depends mainly on the coupling of the laser spike with the extended corona surrounding the imploding shell, where an efficient laser absorption, able to generate a strong shock wave ($> 300\,\mathrm{Mbar}$), is needed. In recent experiments carried out at OMEGA laser [12,13] in spherical irradiation geometry, at laser intensities relevant for SI ($I \sim 6 \times 10^{15}\,\mathrm{W/cm^2}$), a peak ablation pressure close to 400 Mbar was inferred, which constitutes a significant breakthrough toward the demonstration of the feasibility of the SI scheme. Despite this step forward, the physics of laser-plasma interaction in this highly non-linear regime, is still largely unknown and needs dedicated investigations.

Notably, laser-plasma interaction at $I\lambda^2 > 10^{14}\,\mathrm{W}\mu\mathrm{m}^2/\mathrm{cm}^2$ is strongly non-linear. Parametric instabilities (Stimulated Brillouin Scattering (SBS), Stimulated Raman Scattering (SRS), and Two-Plasmon

Decay (TPD)) may arise [14–17], with the unwanted effects of reflecting a large part of incident laser light and generating Hot Electrons (HEs). Further, laser filamentation may alter compression uniformity and enhance the growth of parametric instabilities [18].

The presence of HEs is usually detrimental in ICF because they may preheat the target, making compression more difficult. In the SI scheme, HEs are generated at the end of the compression phase, when the shell areal density is high. As a result, they do not affect target compression and might even improve the shock pressure provided their kinetic energy is not too large [1,12,13,19]. However, recent studies using a hydrodynamic model incorporating HEs effects [20] suggest that the highest energy HEs may prevent hotspot ignition by preheating the fuel and by driving an inner-shell interface ablation that increases the hotspot mass prior to the ignitor shock arrival [21]. As such, the characterization of HEs generated in the SI regime is a key physical issue that must be carried out.

While integrated SI experiments require spherical geometry, many underlying processes can be investigated in planar geometry, which offers the advantage of a simpler scheme and an easier approach to diagnostics. In this letter, we report experimental results in the intensity range (2–6) $\times 10^{15}\,\mathrm{W/cm^2}$, obtained using the Prague Asterix Laser System (PALS) [22], and simulation results obtained with the radiative-hydrodynamic code CHIC [23] that includes a description of the non-linear laser-plasma interaction. While in previous work [24] we investigated hydrodynamics and shock propagation, here we focus on the impact of laser-plasma instabilities and their role in the generation of hot electrons. Although plasma conditions are significantly different from those envisaged in a real SI reactor, in particular density scale length and electron temperature are lower than expected, we think that the data reported here can contribute to draw a picture of the growth of parametric instabilities in this interaction regime. Our work shows that the impact of parametric instabilities in the SI regime is controlled by local intensities and plasma conditions, varying on the scale of speckle dimensions, which can drive non-linear and kinetic effects. An accurate modeling of the local interaction is therefore needed in order to allow mastering the interaction and hence the processes bringing to successful shock ignition.

Experimental set-up. – The PALS iodine laser delivers pulses with wavelength $\lambda_0 = 1.3\,\mu$m and duration $\tau = 300\,$ps [22]. In the experiment we used an *auxiliary* pulse delivering $\approx 30\,$J and the *main* pulse delivering up to 300 J, both smoothed with Random Phase Plates (RPP) to produce a uniform irradiation. The auxiliary pulse was operating at the fundamental frequency and focused to $I \approx 7 \times 10^{13}\,\mathrm{W/cm^2}$ in an extended spot (full width at half-maximum, FWHM = $900\,\mu$m) to create an approximately planar plasma. The main pulse, delayed up to 1.2 ns with respect to the auxiliary pulse, was converted to 3ω ($\lambda_0 = 438\,$nm) and focused by an $F/2$ lens to create a strong shock. The beam profile in the laser waist and the effective energy enclosed in it were accurately measured by imaging and calorimetric techniques. A spot size of $100\,\mu$m FWHM provided an envelope peak intensity on the target up to $I_{max} = 6 \times 10^{15}\,\mathrm{W/cm^2}$. Local intensity in laser speckles can however exceed this value by a factor up to one order of magnitude. By changing the delay between the pulses we tuned the density scale length $L = n_e/(\mathrm{d}n_e/\mathrm{d}x)$ of the preformed plasma. According to hydrodynamic simulations, L varies from 50 to $150\,\mu$m in the underdense plasma during the interaction with the main pulse. These values are in agreement with interferometric measurements conducted both in the visible [25] and in the X-ray domain [26].

Three-layer targets were used. The front layer was parylene-C plastic (C_8H_7Cl) of various thicknesses, mimicking a low-Z ICF ablator material. High-resolution X-ray spectroscopy of chlorine ions allowed getting the plasma temperature [26]. Underneath plastic, two tracer layers of Ti and Cu ($10\,\mu$m each) were placed. X-ray spectroscopy of Ti and Cu K_α radiation, originating from collisions with hot electrons, was used to estimate their average energy and flux. K_α emission was measured with a CCD working in single-photon regime and with two spherically bent quartz (422) and (203) crystals providing a 2D spatial distribution of K_α intensity on the target surface [27]. Both K_α and X-ray spectrometers used Kodak AA400 films as detectors.

The backscattered radiation from SRS and SBS was collected through the focusing lens of the main beam and measured by two calorimeters. On the same line, backscattered radiation was spectrally analyzed by a broadband spectrometer, allowing the detection of radiation both in the range $\omega_0/2 < \omega < \omega_0$, originating from SRS at $n_e < n_c/4$, and at $\omega \approx \omega_0/2$, originating from SRS/TPD occurring at $n_e \approx n_c/4$. Besides, the $3/2\omega_0$ harmonic of the laser frequency, generated by the mixing of laser light with electron plasma waves (EPWs) produced by TPD, was collected inside the vacuum chamber and sent to a UV spectrometer and a calorimeter.

Experimental results. –

X-ray spectroscopy. X-ray spectra, showing well-resolved He- and Li-like lines from Cl ions, were compared with SPECT3D [28] predictions, providing a time-integrated temperature of $\approx$ 700–850 eV in the overdense plasma near the ablation surface ($n_e \approx 3n_{cr} \approx 2 \times 10^{22}\,\mathrm{cm^3}$) [26]. This temperature is in a good agreement with hydrodynamic simulations and, as expected, is lower than in the underdense region ($n_e \approx n_c/4$), as inferred from the $\omega_0/2$ spectra (see below).

Calorimetry. Back-reflected light is dominated by wavelengths near $\lambda \approx 438\,$nm, carrying 5–15% of the incident energy and originating from SBS and laser light reflected at the critical density. The light backscattered by SRS, in the 630–750 nm range, is $\sim$ 0.02–0.2% of the laser

energy. The energy backscattered in both spectral ranges increases when the delay rises from 0 to 1200 ps, growing by a factor 2 and 5, respectively. Indeed, larger delays produce longer scale length plasmas, resulting in larger gain for instabilities. The estimated energy scattered in half-harmonics is $\sim 0.5\%$ of laser light. These values are larger than what reported in our previous paper [24] due to a more accurate characterization of the laser intensity profile in the focal plane. Our new evaluation is closer to data from other experiments [2]. The use of an integrating sphere also showed the presence of light scattered outside the lens focusing cone.

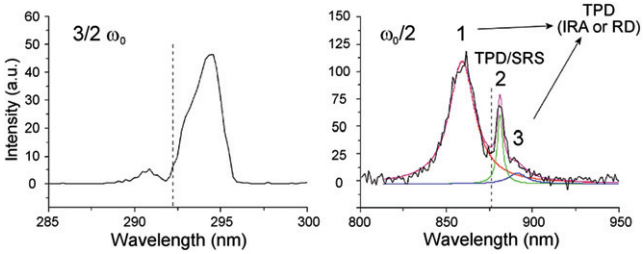

Fig. 1: (Colour online) Typical $3/2\omega_0$ and $\omega_0/2$ spectra, obtained at $5 \times 10^{15}\,\mathrm{W/cm^2}$.

Two-plasmon decay. Emission of $3/2\omega_0$ and $\omega_0/2$ harmonics was detected, giving evidence that a fraction of laser radiation reaches the $n_c/4$ surface. Both components show a doublet structure (see fig. 1), related to the frequency difference of plasma waves produced by TPD instability $|\delta\omega|/\omega_0 = (9/4)(\nu_e^2/c^2)\kappa$, where $\kappa = \boldsymbol{k}_e \cdot \boldsymbol{k}_0/k_0^2 - 1/2$, $\boldsymbol{k}_e$ is the blue EPW wave vector and v_e is the electron thermal velocity. The $3/2\omega_0$ harmonic ($\lambda = 292\,\mathrm{nm}$) blue peak is weaker than the red one, due the fact that the blue EPW must be reflected at the critical density before coupling to the laser light.

Spectra of the $\omega_0/2$ harmonic ($\lambda = 876\,\mathrm{nm}$) agree with the results of other experiments [29,30], showing a broad blue-shifted peak (labeled 1), a sharp red-shifted peak (2), and a less evident small bump at even higher wavelengths (3), which in ref. [30] is referred to as a supplementary peak. The blue peak 1 has a shift similar to peak 3, and approximately 3 times the shift of the narrow red peak 2. Also the width of peak 1 is larger (~ 3.6 times) than that of peak 2, suggesting a different origin. The sharp red-shifted peak 2 is associated to hybrid TPD/SRS instability [31], as in ref. [30], where the laser wave decays into a forward EPW with wave vector $\boldsymbol{k}_e \approx \boldsymbol{k}_0$ ($\kappa = 1/2$) and in a backward partly electrostatic and partly electromagnetic wave. Peaks 1 and 3 are associated to TPD waves and are produced by Inverse Resonance Absorption (IRA) or Raman Downscattering (RD) of laser light [32]. In the IRA process, an EPW with $k_\perp/k_0 < 0.1$ is converted into a photon near its turning point. Considering that blue EPWs propagate inward the density gradient, *i.e.*, toward their turning point, it is expected that the $\omega_0/2$ blue peak is more intense than the red one, that is originated by outgoing EPWs and need additional processes (*e.g.*, Langmuir decay instability) to reverse their direction and be converted into photons. In the RD process, conversely, a laser photon is downscattered by a plasmon produced by TPD. The matching conditions for this process however need that the laser photon is rescattered at a proper angle or that the photon is produced by stimulated Brillouin scattering, as shown in detail in refs. [30,32]. So, both IRA and RD need particular coupling conditions, and many authors have speculated on the prevalence of the one or the other in different experiments. Here, both coupling conditions can be fulfilled near $n_c/4$, where filamentation, turbulence, cavitation and laser photon scattering can occur.

According to ref. [30], the shift of the narrow peak 2 in the $\omega_0/2$ spectrum provides a reliable estimate of plasma temperature not being affected by the observation angle, filamentation or cavitation [33]. By setting $\kappa = 1/2$, we find that the plasma temperature increases from 1.35 to 1.68 keV when I_{max} rises from 2.4 to $3.7 \times 10^{15}\,\mathrm{W/cm^2}$. This agrees with hydrodynamic simulations and with the Landau cutoff of SRS produced at densities $n_e < n_c/4$.

Interestingly, the frequency shift of the peaks of $3/2\omega_0$ emission, $\overline{\Delta\omega}/\omega_0 \approx 1.1 \times 10^{-2}$, is equal to that of peaks 1 and 3 of the $\omega_0/2$ spectrum, suggesting that the EPWs responsible for these harmonics are the same ($k_e \approx 2.9 k_0$). For a plasma temperature $T_e \approx 1.5\,\mathrm{keV}$, we get $k_e\lambda_D \approx 0.27$, indicating that these EPWs are close to the Landau cutoff.

Stimulated Raman scattering. Typical SRS spectra are shown in fig. 2(a), revealing a backscattered emission in the spectral range 630–750 nm. Wave number matching conditions locate backward SRS in the 0.09–0.16 n_c density range, well below $n_c/4$. The short-wavelength limit corresponds to the expected Landau cutoff ($k\lambda_D \approx 0.27$) for the electron temperature of $\sim 1.5\,\mathrm{keV}$.

Spectra also exhibit complex and non-reproducible features, where intensity, spectral bandwidth and complexity strongly increase with the laser intensity and the delay. Since the intensity threshold for SRS in a non-uniform plasma scales inversely with the density scale-length L, and the SRS growth rate γ_0^2 is proportional to the laser intensity I, we then plotted the spectrally integrated intensity I_{SRS} *vs.* the product $I \cdot L$ (fig. 2(b)). Given the time and space dependence of laser intensity, we considered the laser intensity I_{av} averaged over one standard deviation in time and space ($I_{av} = I_{max}/1.366$). L values for the different shot conditions (intensity, delay) were taken from hydrodynamic simulations. Figure 2(b) shows a typical SRS feature of exponential growth leveling off at saturation, which is hidden in the plot as a function of laser intensity alone (not shown here). This is the indication that the density gradient is indeed decisive in determining the SRS growth.

According to ref. [34], the SRS threshold intensity I_{th} in inhomogeneous plasmas is given by

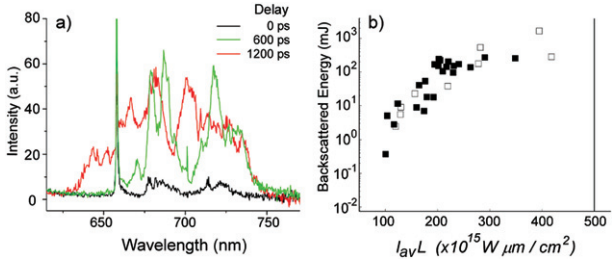

Fig. 2: (Colour online) (a) Backscattered SRS emission spectra obtained with laser intensity $I \approx 4 \times 10^{15}$ W/cm^2 and different delays between prepulse and main pulse (0, 600, and 1200 ps). The spike at 657 nm is a laser harmonic. (b) Backscattered SRS energy *vs.* the product $I_{av} \cdot L$, where I_{av} is the average laser intensity. Full squares are experimental data and empty squares hydrodynamic simulations. The vertical line represents the SRS threshold.

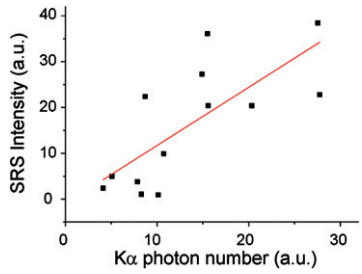

Fig. 3: (Colour online) Correlation between K_α photon number, generated from collisions with hot electrons, and SRS intensity.

$v_0^2/c^2 > 4|\boldsymbol{k}_e - \boldsymbol{k}_0|/k_e^2 L$, where v_0 is the quiver velocity of an electron in the laser field.

This condition implies that $I_{th} \cdot L = 500 \times 10^{15}$ Wμm/cm^2 (vertical line in fig. 2(b)), corresponding to a threshold intensity I_{th} between 4.5×10^{15} and 8×10^{15} W/cm^2, depending on the density scale length, which is above the intensity in all our shots. This suggests that SRS is originated into the laser speckles, and the intensity statistics across the RPP-smoothed laser beam is essential for explaining our results. Based on the focusing geometry and focal volume size, the number of speckles can be estimated to be $\approx 10^5$. Assuming an exponential speckle intensity distribution $f(I) \propto \exp(-I/I_{av})/I_{av}$ typical for RPP-smoothed beams [35], intensities up to $\sim$ 8–10I_{av} can be achieved. Moreover, the most intense speckles can undergo self-focusing further contributing to the SRS emission. At the lowest laser intensities, only speckles with intensities at least ≥ 5 times the average intensity can drive SRS. Conversely, at higher laser intensities, also speckles with intensity marginally higher than I_{av} can play a role. Therefore, when the laser intensity increases, SRS reflectivity increases as the result both of the larger intensity in a single speckle, and of the increasing number of speckles above I_{thres}. This trend is confirmed by numerical simulations as explained in detail below (empty symbols in fig. 2(b)). Nevertheless, the growth observed in the experiment is smaller than that expected by the Rosenbluth gain [36]. This suggests that damping and kinetic effects lead to saturation of SRS inside the speckles. The importance of kinetic mechanisms in SRS saturation is also suggested by the spectral broadening shown in fig. 2(a), increasing with intensity and delay. This can be related to temporal reflectivity bursts and pulsations in non-linear saturation of anomalous SRS, as found in kinetic (PIC) simulations [33,37].

Hot electrons. HEs flux and average energy were obtained by Cu K_α and Ti K_α spectroscopy. The reduction of the K_α yield obtained by increasing the plastic thickness allowed the penetration depth of HEs to be calculated and hence their average energy. Another approach for estimating the HE energy is to consider the ratio between Cu K_α and Ti K_α emissions on the same shot, which is more accurate since this value does not depend on the absolute number of generated hot electrons. Monte Carlo simulations performed with the GEANT4 [38] and PENELOPE [39] codes were used for evaluating the hot-electron temperature, by using the electron stopping range tables [40]. Assuming an exponential distribution for hot electrons $\sim \exp(-E/T_{hot})$, the average energy ("temperature") is found to be $T_{hot} = 25 \pm 8$ keV and the energy conversion $\sim 0.1\% \pm 0.05\%$ of the incident laser energy. Such values are in agreement with data obtained from plasmas with similar temperature and density scale length values, where SRS is the main source of HEs [41]. Also, the HE energy is close to what can be estimated from the phase velocity of the SRS-driven plasma waves in the density region 0.09–0.16 n_c, which is $T_{SRS} \sim$ 17–20 keV. These arguments suggest that HEs are mainly generated by SRS, and only marginally by TPD. This conclusion is also supported by the coarse correlation between Cu K_α photon number and SRS signal (fig. 3).

Numerical simulations. – Simulations have been carried out using the radiative-hydrodynamic code CHIC [23]. In addition to laser refraction, diffraction, resonant and collisional absorption, the code takes into account SRS and TPD processes and generation of HEs, by means of appropriate scaling laws using the local and instantaneous values of laser intensity and plasma parameters [20]. Since SBS was not included in the model, the related reflected energy was subtracted from the incident pulse. The LPI-generated HEs are transported into the plasma using a reduced model based on the angular scattering approximation [42,43], validated against kinetic simulations. This coupled approach allows accounting for the interplay between HEs energy deposition, hydrodynamics and competition between LPI processes.

In this code, laser propagation is described using a new model based on stochastically distributed Gaussian beamlets [44]. This allows reproducing the laser intensity envelope and, to a significant extent, the speckles in the focal spot. Typically, the model is able to reproduce realistic intensity distributions up to 4–5I_{av} but not the

speckles of higher intensity, a limitation imposed by the mesh size. According to the expected intensity distribution in the speckles, the energy fraction contained in speckles above $5I_{av}$ (noted χ_5) is only 0.67%. Nonetheless, these high-intensity speckles may play an important role in our experimental conditions (fig. 2(b)). We addressed this issue in the simulations by maximizing the energy fraction χ_5, within the limits of the laser propagation model. This was obtained by refining the Lagrangian mesh to allow for smaller scale variations of the intensity distribution. Mesh refinement in the code allowed to reach values of $\chi_5 \approx 0.3\%$. The difference between this value and that expected in the experiment ($\chi_5 \approx 0.67\%$) was compensated by using a value of SRS threshold lower than the calculated one by a factor of 2. The same mesh resolution and modified threshold were then used for all simulations.

In order to test the validity of our model, we ran simulations at intensities well below the modified threshold ($I_{av} = 2.1 \times 10^{15}\,\mathrm{W/cm^2}$). An increase of χ_5 from 0.02% to 0.06% and 0.3% with reduced SRS threshold resulted in a SRS signal increase from the noise level (*i.e.*, no SRS predicted) to 0.003% and 0.008% of the incident laser energy. The latter value reasonably matches the experimental results, while the increasing trend of SRS with χ_5 clearly shows the impact of the intensity statistics on the SRS level.

Simulations accounting for the speckle statistics were carried out in our experimental conditions, where the envelope laser intensity is significantly lower than the SRS threshold. A good agreement is obtained (empty squares in fig. 2(b)) confirming the importance of accurate modeling of the speckle statistics.

A general picture of the interaction can be drawn by inspecting simulation results obtained at a laser intensity of $4 \times 10^{15}\,\mathrm{W/cm^2}$ and with a 600 ps delay between the pulses. A large fraction of the pulse energy is collisionally absorbed (∼70.5%) while a small amount (∼1.3%) is resonantly absorbed at the critical surface. The resonant absorption produces electrons with an average energy of ∼3 keV, which are therefore indistinguishable from the thermal electrons. SRS and TPD appear slightly later. The time-integrated SRS reflectivity is ∼ 0.25%, in good agreement with the experiment. Both TPD and SRS produce forward emitted HEs, with conversion efficiencies of ∼ 0.35% and 0.07% of the laser energy, respectively. The temperature of hot electrons from TPD (≈ 66 keV) is higher than that of electrons from SRS (≈ 17 keV), as expected. The measured HEs temperature is between these two values but definitely closer to SRS. The discrepancy in HE production from TPD in the simulation suggests that, in the experiment, TPD is damped or saturated by kinetic effects. Since in our model, parametric instabilities are described by scaling laws, saturation processes specific for our conditions (*e.g.*, cavitation phenomena or damping of daughter waves into small speckles) are probably underestimated.

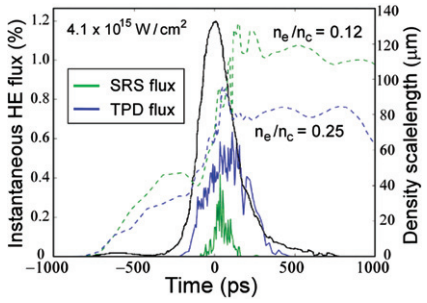

Fig. 4: (Colour online) Instantaneous HE flux as a function of time for SRS (green) and TPD (blue). Density scale lengths computed at $n_c/4$ and $0.12n_c$ are also shown (dashed blue and green lines, respectively). The peak intensity of the laser pulse is indicated as a gray line.

The evolution of the density scale length at $n_e \approx 0.12n_c$ and $n_e \approx n_c/4$, indicative, respectively, of the layers where SRS and TPD are active, is shown in fig. 4 alongside the laser/HE energy conversion efficiencies. SRS is maximum after the laser peak, when the scalelength becomes large enough while the laser intensity remains high. The plasma temperature is similar in both layers and varies with time from 0.5 to 2.8 keV at the laser peak. This is in good agreement with the time-integrated estimate based on TPD splitting ($T_e \approx 1.68\,\mathrm{keV}$ at $I = 3.7 \cdot 10^{15}\,\mathrm{W/cm^2}$). In the overdense region, the plasma temperature is lower, in agreement with X-ray spectroscopy results.

Summary and conclusions. – In the present experiment, backscattering is dominated by SBS and laser reflection (5–15%) while the contribution from SRS, occurring at 0.09–$0.16n_c$ near the Landau cutoff, is of the order of 0.1%. While the level of SBS agrees with other experiments carried out under similar interaction conditions, SRS backscatter appears at least an order of magnitude lower [12,41,45]. This can be maybe explained by the longer plasma scale lengths obtained in other works and/or by the low $f/\#$ of our focussing system, that combined with the phase plate, results in small speckles, inhibiting filamentation and damping the SRS growth.

The latter seems confirmed by the spectral modulation of SRS spectra and the reflectivity saturation observed at the highest laser intensities/delays explored, which suggests the occurrence of kinetic effects suppressing the growth of EPWs inside the speckles. The correlation of SRS reflectivity and K_α emission and the measured HE temperature (25 keV) suggest that HEs are mainly generated by SRS, similarly to conclusions of recent experiments in spherical geometry [12,41]. The presence of half-harmonics confirms the TPD at $n_c/4$.

Hydrodynamic simulations well reproduce SRS levels and the plasma temperature from the experiment, while TPD is overestimated, probably because saturation mechanisms are underestimated. The agreement of simulated and experimental SRS reflectivities points out the need

of correctly modeling the speckle intensity statistics for reproducing LPI in laser-fusion experiments.

* * *

This work was supported by the European Union under the Laserlab program of the 7th FP and the COST Action MP1208, by the Czech Ministry of Education, Youth and Sports, projects LC528 and LM2010014, by the Italian MIUR (contract PRIN 2012AY5LEL), by the EUROfusion Consortium (grant agreement 633053), by the Sapienza project C26A15YTMA and by the ELI project CZ.02.1.01/0.0/0.0/15 008/0000162 from European Regional Development Fund. SciTech Precision supplied targets. The authors are grateful the PALS staff for help in running the experiments.

REFERENCES

[1] Betti R. *et al.*, *Phys. Rev. Lett.*, **98** (2007) 155001.
[2] Batani D. *et al.*, *Nucl. Fusion*, **54** (2014) 054009.
[3] Perkins L. J. *et al.*, *Phys. Rev. Lett.*, **103** (2009) 045004.
[4] Ribeyre X. *et al.*, *Plasma Phys. Control. Fusion*, **51** (2009) 015013.
[5] Atzeni S. *et al.*, *Plasma Phys. Control. Fusion*, **53** (2011) 035010.
[6] Atzeni S. *et al.*, *Nucl. Fusion*, **54** (2014) 054008.
[7] Nuckolls J. *et al.*, *Nature*, **239** (1972) 139.
[8] Lindl J., *Phys. Plasmas*, **2** (1995) 3933.
[9] Atzeni S. and Meyer-ter-Vehn J., *The Physics of Inertial Fusion* (Clarendon-Oxford) 2004.
[10] Theobald W. *et al.*, *Plasma Phys. Control. Fusion*, **51** (2009) 124052.
[11] Anderson K. S. *et al.*, *Phys. Plasmas*, **20** (2013) 056312.
[12] Theobald W. *et al.*, *Phys. Plasmas*, **22** (2015) 056310.
[13] Nora R. *et al.*, *Phys. Rev. Lett.*, **114** (2015) 045001.
[14] Kruer W. L., *The Physics of Laser Plasma Interactions* (Addison-Wesley, Redwood City, Cal.) 1988.
[15] Seka W. *et al.*, *Phys. Fluids*, **27** (1984) 2181.
[16] Afshar-rad T. *et al.*, *Phys. Rev. Lett.*, **68** (1992) 942.
[17] Tanaka K. *et al.*, *Phys. Rev. Lett.*, **48** (1982) 1179.
[18] Giulietti A. *et al.*, *Phys. Rev. E*, **59** (1999) 1038.
[19] Ribeyre X. *et al.*, *Phys. Plasmas*, **20** (2013) 062705.
[20] Colaïtis A. *et al.*, *Phys. Rev. E*, **92** (2016) 041101.
[21] Colaïtis A. *et al.*, *Phys. Plasmas*, **23** (2016) 072703.
[22] Jungwirthv K. *et al.*, *Phys. Plasmas*, **8** (2001) 2495.
[23] Breil J. *et al.*, *Comput. Fluids*, **46** (2011) 161.
[24] Batani D. *et al.*, *Phys. Plasmas*, **21** (2014) 032710.
[25] Pisarczyk T. *et al.*, *Phys. Plasmas*, **21** (2014) 012708.
[26] Šmíd M. *et al.*, *Acta Polytech.*, **53** (2013) 233.
[27] Morace A. and Batani D., *Nucl. Instrum. Methods A*, **623** (2010) 797.
[28] MacFarlane J. J. *et al.*, *High Energy Density Phys.*, **3** (2007) 181.
[29] Seka W. *et al.*, *Phys. Plasmas*, **16** (2009) 052701.
[30] Seka W. *et al.*, *Phys. Fluids*, **28** (1985) 2570.
[31] Afeyan B. B. and Williams E. A., *Phys. Rev. Lett.*, **75** (1995) 4218.
[32] Berger R. L. and Powers L. V., *Phys. Fluids*, **28** (1985) 2895.
[33] Klimo O. and Tikhonchuk V. T., *Plasma Phys. Control. Fusion*, **55** (2013) 095002.
[34] Forslund D. W. *et al.*, *Phys. Fluids*, **18** (1975) 1002.
[35] Rose H. A. and Dubois D. F., *Phys. Fluids B*, **5** (1993) 590.
[36] Rosenbluth M. N., *Phys. Rev. Lett.*, **29** (1972) 565.
[37] Klimo O. *et al.*, *Plasma Phys. Control. Fusion*, **56** (2014) 055010.
[38] Sempau J. *et al.*, *Nucl. Instrum. Methods B*, **132** (1997) 377.
[39] Agostinelli S. *et al.*, *Nucl. Instrum. Methods A*, **506** (2003) 250.
[40] `http://physics.nist.gov/PhysRefData/Star/Text/ESTAR.html`.
[41] Theobald W. *et al.*, *Phys. Plasmas*, **19** (2012) 102706.
[42] Li C. K. and Petrasso R. D., *Phys. Rev. E*, **70** (2004) 067401.
[43] Solodov A. A. and Betti R., *Phys. Plasmas*, **15** (2008) 042707.
[44] Colaïtis A. *et al.*, *Phys. Rev. E*, **89** (2014) 033101.
[45] Baton S. D. *et al.*, *Phys. Rev. Lett.*, **108** (2012) 195002.